

# Precise predictions for $h_a \rightarrow h_b h_c$ decays in the complex MSSM

K.E. WILLIAMS\* AND G. WEIGLEIN†

*IPPP, University of Durham, Durham DH1 3LE, UK*

## Abstract

Complete one-loop results for the decay widths of neutral Higgs bosons ( $h_a$ ) into lighter neutral Higgs bosons ( $h_b, h_c$ ) are presented for the MSSM with complex parameters. The results are obtained in the Feynman-diagrammatic approach, taking into account the full dependence on the spectrum of supersymmetric particles and all complex phases of the supersymmetric parameters. The genuine triple-Higgs vertex contributions are supplemented with two-loop propagator-type corrections, yielding the currently most precise prediction for this class of processes. The genuine vertex corrections turn out to be very important, yielding a large increase of the decay width compared to a prediction based on the tree-level vertex. The new results are used to analyse the impact of the experimental limits from the LEP Higgs searches on the parameter space with a very light MSSM Higgs boson. It is found that a significant part of the parameter space of the CPX benchmark scenario exists where channels involving the decay  $h_2 \rightarrow h_1 h_1$  have the highest search sensitivity, and the existence of an unexcluded region with  $M_{h_1} \approx 45$  GeV is confirmed.

---

\*email: K.E.Williams@durham.ac.uk

†email: Georg.Weiglein@durham.ac.uk

# 1 Introduction

Higgs self-couplings, i.e. triple-Higgs couplings,  $h_a h_b h_c$ , and quartic Higgs couplings,  $h_a h_b h_c h_d$ , are a crucial element of electroweak symmetry breaking via the Higgs mechanism. While the prospects for a direct experimental determination of the quartic Higgs coupling at present and future colliders are small (see e.g. Ref. [1]), probing the triple-Higgs coupling will be one of the prime goals in the experimental programme for testing the Higgs mechanism. This coupling can be accessed via a precision measurement of the Higgs production process  $e^+e^- \rightarrow Zh_a h_a$  at the ILC [2] or CLIC [3], and via Higgs cascade decays of the form  $h_a \rightarrow h_b h_c$ . While Higgs cascade decays are obviously impossible in the Standard Model (SM), they can play an important role in models with extended Higgs sectors.

Besides the interest in Higgs cascade decays as a means to directly probe Higgs self-couplings, a precise prediction for decays of this kind is also important for phenomenological reasons. Where kinematically possible the Higgs cascade decay modes can even be dominant and affect Higgs phenomenology very significantly.

A well-known example of an extended Higgs sector is the Minimal Supersymmetric Standard Model (MSSM), whose Higgs sector comprises two scalar doublets that accommodate five physical Higgs bosons. In lowest order these are the light and heavy  $\mathcal{CP}$ -even  $h$  and  $H$ , the  $\mathcal{CP}$ -odd  $A$ , and the charged Higgs bosons  $H^\pm$ . Higher-order contributions yield large corrections to the masses and couplings, and also induce  $\mathcal{CP}$ -violation leading to mixing between  $h, H$  and  $A$  in the case of general complex SUSY-breaking parameters. The corresponding mass eigenstates are denoted as  $h_1, h_2, h_3$ . If the mixing between the three neutral mass eigenstates is such that the coupling of the lightest Higgs boson to gauge bosons is significantly suppressed, this state can be very light without being in conflict with the exclusion bounds from the LEP Higgs searches [5]. In this case the second-lightest Higgs boson,  $h_2$ , may predominantly decay into a pair of light Higgs bosons,  $h_2 \rightarrow h_1 h_1$ .

The results of the Higgs searches at LEP [4, 5] have been interpreted in certain MSSM benchmark scenarios [6, 7]. In the CPX scenario [7], which involves large complex phases of the trilinear coupling,  $A_t$ , and the gluino mass parameter,  $M_3$ , the decay  $h_2 \rightarrow h_1 h_1$  is important in a significant part of the parameter space. This decay mode leads to a quite complicated final state, corresponding to a 6-jet topology if  $h_2$  is produced in association with an hadronically decaying  $Z$  boson or in association with  $h_1$ . In the analysis of the LEP Higgs searches within the CPX scenario an unexcluded region for light  $h_1$  and relatively small values of  $\tan\beta$  (the ratio of the vacuum expectation values of the two Higgs doublets) remained, so that no firm lower bound on the mass of the lightest Higgs boson of the MSSM could be set. The unexcluded parameter region with a very light Higgs boson will also be difficult to cover with the Higgs searches at the LHC [1, 8, 9] (see also Ref. [10] for a recent study).<sup>1</sup>

In order to reliably determine which parameter regions of the MSSM with a very light

---

<sup>1</sup> It should be noted that Higgs cascade decays are possible in the MSSM also in the limit where complex phases are neglected. The decay  $h \rightarrow AA$  occurs in a small parameter region with very light  $M_A$  [11], leading to small unexcluded parameter regions in the  $M_A$ - $\tan\beta$  plane from LEP Higgs searches [5] (especially in the “no-mixing” scenario [6]). For large values of  $M_A$  also the decay  $H \rightarrow hh$  can occur. Higgs cascade decays into very light Higgs bosons can also be important in a considerable part of the parameter space of extensions of the MSSM, see e.g. Ref. [12] for a discussion within the NMSSM.

Higgs boson are unexcluded by the Higgs searches so far and which regions will be accessible by Higgs searches in the future, precise predictions for the Higgs cascade decays  $h_a \rightarrow h_b h_c$  in the MSSM with complex parameters (cMSSM) are indispensable. For propagator-type corrections the evaluations are quite advanced, and results incorporating the dominant one- and two-loop contributions have been obtained within the Feynman-diagrammatic (FD) approach [13–15] and the renormalisation-group (RG) improved effective potential approach [16]. The public codes *FeynHiggs* [14, 15, 17, 18], based on the FD approach, and *CPsuperH* [19], based on the RG improved effective potential approach, are available. For the genuine  $h_a h_b h_c$  vertex contributions, on the other hand, so far only effective coupling approximations have been available in the cMSSM.

In this paper we obtain complete one-loop results within the FD approach for the decays  $h_a \rightarrow h_b h_c$  taking into account the full dependence on all complex phases of the supersymmetric parameters. The mixing of the three neutral Higgs bosons among themselves and with the  $Z$  boson and the unphysical Goldstone-boson degree of freedom are consistently taken into account. We furthermore obtain complete one-loop results for the decays of neutral Higgs bosons into SM fermions in the cMSSM,  $h_a \rightarrow f\bar{f}$ . The new one-loop results are combined with all existing higher-order corrections in the FD approach, yielding in this way the currently most precise predictions for the class of processes  $h_a \rightarrow h_b h_c$ . The results presented in this paper will be included in the code *FeynHiggs* [14, 15, 17, 18]. We find that the genuine vertex corrections are very important for a reliable prediction of the Higgs cascade decays. The genuine vertex corrections lead to a drastic change compared to a prediction taking into account propagator-type corrections only. We compare our full result with various approximations and investigate the dependence on the complex phases. As an application of our improved theoretical predictions, we analyse to what extent the previously unexcluded parameter region with a rather light Higgs boson is compatible with the limits on topological cross sections obtained from the LEP Higgs searches.

## 2 The MSSM with complex parameters: notations and conventions

The MSSM, in its most general form, contains  $\mathcal{CP}$ -violating phases at tree level in the Higgs, slepton, squark, chargino/neutralino and gluino sectors. The gauge-boson, lepton and quark sectors do not contain extra phases (we assume in this paper a unit CKM matrix). In our calculation the full dependence on all complex phases of the supersymmetric parameters is taken into account. In the following we briefly specify the notations and conventions used in this paper and define the parameters that are relevant for the discussion of the numerical results.

### 2.1 The squark sector

The bilinear terms of the squarks in the Lagrangian give rise to the mass matrix

$$M_{\tilde{q}} = \begin{pmatrix} M_L^2 + m_q^2 + M_Z^2 \cos 2\beta (I_3^q - Q_q s_w^2) & m_q X_q^* \\ m_q X_q & M_{qR}^2 + m_q^2 + M_Z^2 \cos 2\beta Q_q s_w^2 \end{pmatrix}, \quad (1)$$

where

$$X_q \equiv A_q - \mu^* \{\cot \beta, \tan \beta\}, \quad (2)$$

and the trilinear couplings  $A_q$  and the Higgs-mixing parameter  $\mu$  can be complex. This mass matrix needs to be diagonalised to get the tree-level physical states  $\tilde{q}_1, \tilde{q}_2$ ,

$$\begin{pmatrix} \tilde{q}_1 \\ \tilde{q}_2 \end{pmatrix} = \begin{pmatrix} c_{\tilde{q}} & s_{\tilde{q}} \\ -s_{\tilde{q}}^* & c_{\tilde{q}} \end{pmatrix} \begin{pmatrix} \tilde{q}_L \\ \tilde{q}_R \end{pmatrix}, \quad (3)$$

where in our conventions  $c_{\tilde{q}}$  is real and  $s_{\tilde{q}}$  is complex.

## 2.2 The neutral Higgs sector

### 2.2.1 Tree level

We write the two Higgs doublets as

$$\begin{aligned} \mathcal{H}_1 &= \begin{pmatrix} H_{11} \\ H_{12} \end{pmatrix} = \begin{pmatrix} v_1 + \frac{1}{\sqrt{2}}(\phi_1 - i\chi_1) \\ -\phi_1^- \end{pmatrix}, \\ \mathcal{H}_2 &= \begin{pmatrix} H_{21} \\ H_{22} \end{pmatrix} = \begin{pmatrix} \phi_2^+ \\ v_2 + \frac{1}{\sqrt{2}}(\phi_2 + i\chi_2) \end{pmatrix}, \end{aligned} \quad (4)$$

where  $v_1$  and  $v_2$  are the vacuum expectation values, and  $\tan \beta \equiv v_2/v_1$ . The conventions used here are the same as in Ref. [14]. The MSSM Higgs sector is  $\mathcal{CP}$ -conserving at lowest order. The tree-level neutral mass eigenstates  $h, H, A$  and the unphysical Goldstone-boson degree of freedom  $G$  are related to the  $\mathcal{CP}$ -even neutral fields  $\phi_1, \phi_2$  and the  $\mathcal{CP}$ -odd neutral fields  $\chi_1, \chi_2$  through a unitary matrix,

$$\begin{pmatrix} h \\ H \\ A \\ G \end{pmatrix} = \begin{pmatrix} -\sin \alpha & \cos \alpha & 0 & 0 \\ \cos \alpha & \sin \alpha & 0 & 0 \\ 0 & 0 & -\sin \beta_n & \cos \beta_n \\ 0 & 0 & \cos \beta_n & \sin \beta_n \end{pmatrix} \begin{pmatrix} \phi_1 \\ \phi_2 \\ \chi_1 \\ \chi_2 \end{pmatrix}. \quad (5)$$

In the renormalisation prescription that we have adopted, the parameter  $\tan \beta$  receives a counterterm, while the mixing angle  $\beta_n$  remains unrenormalised. After the renormalisation has been carried out, one can set  $\beta_n = \beta$ .

### 2.2.2 Higgs mass matrix in higher orders

To find the loop-corrected neutral Higgs masses, the poles of the  $3 \times 3$  propagator matrix  $\Delta(p^2)$  in the  $(h, H, A)$  basis need to be found (mixing with the Goldstone boson  $G$  and the  $Z$  boson can be neglected in the propagator matrix since the corresponding contributions are of sub-leading two-loop order, see the discussion in Ref. [14]). Determining the poles of the propagator matrix is equivalent to finding the three solutions to

$$\frac{1}{|\Delta(p^2)|} = 0. \quad (6)$$

The propagator matrix is related to the  $3 \times 3$  matrix of the irreducible renormalised 2-point vertex-functions  $\hat{\Gamma}_2(p^2)$  through

$$[-\Delta(p^2)]^{-1} = \hat{\Gamma}_2(p^2) = i [p^2 \mathbb{1} - \mathbf{M}(p^2)], \quad (7)$$

where

$$\mathbf{M}(p^2) = \begin{pmatrix} m_h^2 - \hat{\Sigma}_{hh}(p^2) & -\hat{\Sigma}_{hH}(p^2) & -\hat{\Sigma}_{hA}(p^2) \\ -\hat{\Sigma}_{hH}(p^2) & m_H^2 - \hat{\Sigma}_{HH}(p^2) & -\hat{\Sigma}_{HA}(p^2) \\ -\hat{\Sigma}_{hA}(p^2) & -\hat{\Sigma}_{HA}(p^2) & m_A^2 - \hat{\Sigma}_{AA}(p^2) \end{pmatrix}. \quad (8)$$

Here  $m_h, m_H, m_A$  are the lowest-order mass eigenvalues, and the  $\hat{\Sigma}_{ij}$  ( $i, j = h, H, A$ ) are the renormalised self-energies. In general, the three solutions  $\mathcal{M}_{h_a}^2$  (with  $h_a = h_1, h_2, h_3$ ) are complex. They can be written as

$$\mathcal{M}_{h_a}^2 = M_{h_a}^2 - i M_{h_a} W_{h_a}, \quad (9)$$

where  $M_{h_a}$  is the (loop-corrected) mass of the respective Higgs boson,  $W_{h_a}$  is its width, and by convention

$$M_{h_1} \leq M_{h_2} \leq M_{h_3}. \quad (10)$$

We calculated the self-energies using an expansion about  $M_{h_a}^2$ ,

$$\hat{\Sigma}_{jk}(\mathcal{M}_{h_a}^2) \approx \hat{\Sigma}_{jk}(M_{h_a}^2) + i \text{Im} [\mathcal{M}_{h_a}^2] \hat{\Sigma}'_{jk}(M_{h_a}^2), \quad (11)$$

with  $j, k = h, H, A$  (as a check of our procedure, each time  $\hat{\Sigma}_{jk}(\mathcal{M}_{h_a}^2)$  was calculated, the next term in the expansion was also explicitly calculated, to ensure it is negligible). To find each solution to Eq. (6), an iterative procedure was used.

### 3 Complete one-loop calculation of Higgs-boson cascade decays and decays into SM fermions

We calculated the full 1PI (one-particle irreducible) one-loop vertex contributions to the processes  $h_a \rightarrow h_b h_c$ , taking into account all sectors of the MSSM and the complete dependence on the complex phases of the supersymmetric parameters. Examples of generic diagrams for one of the contributing topologies are shown in Fig. 1.

In order to obtain precise predictions for the branching ratios  $\text{BR}(h_a \rightarrow h_b h_c)$  it is important to calculate also the decay widths of the Higgs bosons into SM fermions,  $h_a \rightarrow f \bar{f}$ , at the same level of accuracy, since the decay modes into  $b \bar{b}$  and  $\tau^+ \tau^-$  are dominant over large parts of the cMSSM parameter space. We therefore derived also complete one-loop results for the processes  $h_a \rightarrow f \bar{f}$  (including SM-type QED and, where appropriate, QCD corrections) for arbitrary values of all complex phases of the supersymmetric parameters. The partial widths for the other Higgs-boson decay modes have been taken from the program *FeynHiggs* [14, 15, 17, 18].

Our calculations have been carried out in the FD approach, making use of the programs *FeynArts* [20] and *FormCalc* [21]. Concerning the renormalisation, we use the same

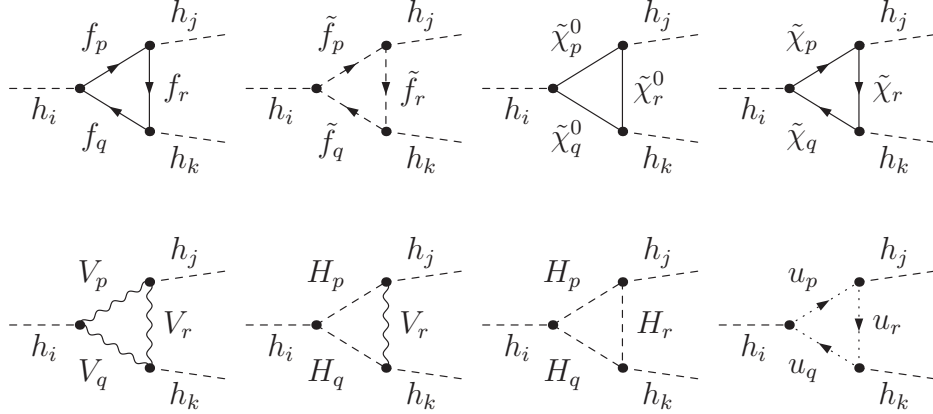


Figure 1: Examples of generic diagrams (showing only one of the topologies) contributing to the processes  $h_i \rightarrow h_j h_k$ , where  $h_i, h_j, h_k = h, H, A$ . Furthermore,  $f$  are SM fermions,  $\tilde{f}$  are their superpartners,  $\tilde{\chi}^0, \tilde{\chi}$  are neutralinos and charginos,  $V$  are vector bosons,  $H$  denote the neutral and charged Higgs bosons and the Goldstone bosons,  $u$  are Faddeev–Popov ghost fields.

transformations and renormalisation conditions as in Ref. [14]. We parameterise the electric charge in the lowest-order decay amplitudes in terms of  $\alpha(M_Z)$ , corresponding to the charge counterterm

$$\frac{\delta e}{e} = \frac{1}{2} \Pi_\gamma(0) - \frac{s_w}{c_w} \frac{\Sigma_{\gamma Z}^T(0)}{M_Z^2} - \frac{1}{2} \Delta\alpha. \quad (12)$$

Here  $\Pi_\gamma(0)$  is the photon vacuum polarisation,  $\Sigma^T$  denotes the transverse part of the self-energy, and  $\Delta\alpha = \Delta\alpha_{\text{had}}^{(5)} + \Delta\alpha_{\text{lept}}$  is the shift in the fine-structure constant arising from large logarithms of light fermions. The other parameter renormalisations are listed in Ref. [14]. The fermion fields in the processes  $h_a \rightarrow f\bar{f}$  are renormalised on-shell. For the renormalisation of the Higgs fields it is convenient to use a  $\overline{\text{DR}}$  scheme as in Ref. [14], while the correct on-shell properties of the S-matrix elements involving external Higgs fields are ensured by the inclusion of finite wave-function normalisation factors.

The wave-function normalisation factors are obtained from

$$Z_h = \frac{1}{\left. \frac{\partial}{\partial p^2} \left( \frac{i}{\Delta_{hh}(p^2)} \right) \right|_{p^2=\mathcal{M}_{h_a}^2}}, \quad Z_H = \frac{1}{\left. \frac{\partial}{\partial p^2} \left( \frac{i}{\Delta_{HH}(p^2)} \right) \right|_{p^2=\mathcal{M}_{h_b}^2}}, \quad Z_A = \frac{1}{\left. \frac{\partial}{\partial p^2} \left( \frac{i}{\Delta_{AA}(p^2)} \right) \right|_{p^2=\mathcal{M}_{h_c}^2}} \quad (13)$$

$$Z_{hH} = \frac{\Delta_{hH}}{\Delta_{hh}} \Big|_{p^2=\mathcal{M}_{h_a}^2}, \quad Z_{Hh} = \frac{\Delta_{hH}}{\Delta_{HH}} \Big|_{p^2=\mathcal{M}_{h_b}^2}, \quad Z_{Ah} = \frac{\Delta_{hA}}{\Delta_{AA}} \Big|_{p^2=\mathcal{M}_{h_c}^2} \quad (14)$$

$$Z_{hA} = \frac{\Delta_{hA}}{\Delta_{hh}} \Big|_{p^2=\mathcal{M}_{h_a}^2}, \quad Z_{HA} = \frac{\Delta_{HA}}{\Delta_{HH}} \Big|_{p^2=\mathcal{M}_{h_b}^2}, \quad Z_{AH} = \frac{\Delta_{HA}}{\Delta_{AA}} \Big|_{p^2=\mathcal{M}_{h_c}^2}, \quad (15)$$

where the  $\Delta_{hh}(p^2)$ ,  $\Delta_{hH}(p^2)$  etc. are the elements of the  $3 \times 3$  Higgs propagator matrix (see

Ref. [14] for expressions in terms of renormalised self-energies), and  $h_a, h_b, h_c$  are some permutation of  $h_1, h_2, h_3$ . For the evaluation of self-energies at complex momenta the expansion in Eq. (11) is employed.

The wave-function normalisation factors can be expressed in terms of a (non-unitary) matrix  $\hat{\mathbf{Z}}$  [14],

$$\hat{\mathbf{Z}} = \begin{pmatrix} \sqrt{Z_h} & \sqrt{Z_h} Z_{hH} & \sqrt{Z_h} Z_{hA} \\ \sqrt{Z_H} Z_{Hh} & \sqrt{Z_H} & \sqrt{Z_H} Z_{HA} \\ \sqrt{Z_A} Z_{Ah} & \sqrt{Z_A} Z_{AH} & \sqrt{Z_A} \end{pmatrix}, \quad (16)$$

where

$$\begin{pmatrix} \hat{\Gamma}_{h_a} \\ \hat{\Gamma}_{h_b} \\ \hat{\Gamma}_{h_c} \end{pmatrix} = \hat{\mathbf{Z}} \cdot \begin{pmatrix} \hat{\Gamma}_h \\ \hat{\Gamma}_H \\ \hat{\Gamma}_A \end{pmatrix}. \quad (17)$$

Here  $\hat{\Gamma}_{h_a}$  is a one-particle irreducible n-point vertex-function (including loop corrections) which involves a single external Higgs boson  $h_a$ .

The matrix  $\hat{\mathbf{Z}}$  fulfills the conditions

$$\lim_{p^2 \rightarrow \mathcal{M}_{h_a}^2} -\frac{i}{p^2 - \mathcal{M}_{h_a}^2} \left( \hat{\mathbf{Z}} \cdot \hat{\Gamma}_2 \cdot \hat{\mathbf{Z}}^T \right)_{hh} = 1 \quad (18)$$

$$\lim_{p^2 \rightarrow \mathcal{M}_{h_b}^2} -\frac{i}{p^2 - \mathcal{M}_{h_b}^2} \left( \hat{\mathbf{Z}} \cdot \hat{\Gamma}_2 \cdot \hat{\mathbf{Z}}^T \right)_{HH} = 1 \quad (19)$$

$$\lim_{p^2 \rightarrow \mathcal{M}_{h_c}^2} -\frac{i}{p^2 - \mathcal{M}_{h_c}^2} \left( \hat{\mathbf{Z}} \cdot \hat{\Gamma}_2 \cdot \hat{\mathbf{Z}}^T \right)_{AA} = 1, \quad (20)$$

where  $\hat{\Gamma}_2$  has been introduced in Eq. (7). We choose in the following  $h_a = h_1$ ,  $h_b = h_2$  and  $h_c = h_3$ . It should be noted that this choice is purely a convention. Other choices would give the same physical results. This fact can most easily be seen if the wave-function normalisation factors are defined as in Eqs. (13)–(15), i.e., with the Higgs-boson self-energies evaluated at the complex pole. In this way the evaluation of the masses and the wave-function normalisation factors is treated on the same footing. The definition of the wave-function normalisation factors adopted in Eqs. (13)–(15) differs slightly from the one in Refs. [14, 22], where the wave-function normalisation factors were defined at the real part of the complex pole (furthermore, in Refs. [14, 22] the real parts of the diagonal wave-function normalisation factors  $Z_h, Z_H, Z_A$  were taken). The two definitions of the wave-function normalisation factors differ by contributions from imaginary parts that are formally of sub-leading two-loop order. It turns out that the inclusion of the imaginary parts improves the numerical stability of the results in certain parameter regions, while otherwise these contributions are completely negligible (see also Ref. [23]).

In a complete one-loop calculation of Higgs decay processes also mixing contributions between the states  $h, H, A$  and the Goldstone and  $Z$  bosons have to be taken into account (we denote these reducible contributions as  $\Gamma_{h_i h_j h_k}^{\text{G,Zmix}}$ ). We treat these mixing contributions strictly at one-loop level in order to ensure the cancellation of unphysical poles (while our



prescription for the wave function normalisation factors described above automatically incorporates leading reducible higher-order contributions). Since the mixing self-energy involving  $G$  and  $Z$  is already a one-loop contribution, in a strict one-loop expansion the  $\Gamma_{h_i h_j h_k}^{G,Z \text{ mix}}$  are evaluated at the (unrotated) tree-level masses  $m_{h_i}^2$ . Accordingly, our results can be written as (summation over repeated indices is understood)

$$\Gamma_{h_a h_b h_c}^{\text{full}} = \hat{\mathbf{Z}}_{ck} \hat{\mathbf{Z}}_{bj} \hat{\mathbf{Z}}_{ai} \left[ \Gamma_{h_i h_j h_k}^{1\text{PI}} (M_{h_a}^2, M_{h_b}^2, M_{h_c}^2) + \Gamma_{h_i h_j h_k}^{G,Z \text{ mix}} (m_{h_i}^2, m_{h_j}^2, m_{h_k}^2) \right] \quad (21)$$

$$\Gamma_{h_a f \bar{f}}^{\text{full}} = \hat{\mathbf{Z}}_{ai} \left[ \Gamma_{h_i f \bar{f}}^{1\text{PI}} (M_{h_a}^2) + \Gamma_{h_i f \bar{f}}^{G,Z \text{ mix}} (m_{h_i}^2) \right], \quad (22)$$

where as before  $h_i, h_j, h_k = h, H, A$ . The numerical impact of the mixing contributions with the Goldstone and  $Z$  bosons on the results presented in this paper turned out to be small.

In our numerical analysis below we will compare our full result with the contribution obtained from the  $t, \tilde{t}$  sector in the approximation where the gauge couplings are neglected and the diagrams are evaluated at zero external momenta. We refer to this approximation as the ‘‘Yukawa Approximation’’, which is expected to yield the leading one-loop contribution if  $\tan \beta$  is not too large. In this approximation, the counterterm contributions in the renormalised vertex all vanish.

## 4 Combination with higher-order results

We have combined our new one-loop result with the most up-to-date higher-order propagator-type contributions in the FD approach. This has been done by supplementing the one-loop self-energies in Eqs. (8) and (13)–(15) with the two-loop self-energies obtained from the program *FeynHiggs* [14, 15, 17, 18]. In *FeynHiggs* the  $\mathcal{O}(\alpha_t \alpha_s)$  corrections are incorporated including the full phase dependence at the two-loop level, while other two-loop contributions so far are only known in the limit of vanishing complex phases [24]. In our numerical analysis below we will restrict to those higher-order contributions for which the phase dependence at the two-loop is explicitly known, i.e. we do not include the residual contributions for which a result exists only in the MSSM with real parameters. The calculation of the decay width  $\Gamma(h_a \rightarrow b\bar{b})$  furthermore contains resummed SUSY-QCD corrections, including the full phase dependence.

By supplementing our complete one-loop results for the processes  $h_a \rightarrow h_b h_c$  and  $h_a \rightarrow f \bar{f}$  with the state-of-the-art higher-order propagator-type corrections we obtain the currently most precise predictions for the  $h_a \rightarrow h_b h_c$  decay widths and branching ratios in the MSSM with complex parameters. It should be noted that in the special case where the complex phases are put to zero our results also provide improved predictions for the Higgs cascade decays occurring in the  $\mathcal{CP}$ -conserving case, i.e.  $h \rightarrow AA$  and  $H \rightarrow hh$ . The numerical impact of the latter will be discussed elsewhere.

In our numerical analysis we also investigated the impact of using loop-corrected Higgs masses and couplings (rather than the tree-level values) within loop diagrams, which is formally a higher-order effect. The numerical impact on our results turned out to be negligible.



## 5 Implementation of exclusion bounds from the LEP Higgs searches

A precise prediction for the process  $h_2 \rightarrow h_1 h_1$  is particularly important for investigating the exclusion bounds from the Higgs searches at LEP [4, 5] within the MSSM with complex parameters. The LEP analysis in the CPX benchmark scenario [7] resulted in an unexcluded parameter region for relatively small  $\tan\beta$  where the lightest neutral Higgs boson is very light but has strongly suppressed couplings to gauge bosons. The second-lightest Higgs boson, on the other hand, may be within the kinematic reach of LEP in this region but has a large branching ratio into a pair of lightest Higgs bosons, i.e.  $h_2 \rightarrow h_1 h_1$ .

In our numerical analysis below we analyse the impact of our new result on the LEP exclusion bounds in the cMSSM. This is done by comparing the cMSSM predictions with the topological cross section limits given in Refs. [4, 5, 25]. The LEP limits on the various cross sections [4, 5] have been implemented into the code *HiggsBounds* [26] (for applications of preliminary versions of *HiggsBounds*, see Ref. [27]). In order to obtain a correct statistical interpretation of the overall exclusion limit at the 95% C.L., the first step is to determine, for each parameter point, which one of the various channels has the highest statistical sensitivity for setting an exclusion limit [25]. We then compare the theoretical prediction for this particular channel with the topological cross section limit determined at LEP for this channel. We neglect, in this analysis, the theoretical uncertainties from unknown higher-order corrections — see Ref. [26] for a discussion of this issue. The predictions of the topological cross sections have been obtained using the wave-function normalisation factors defined in Sect. 3.

While the topological cross section limits are very convenient for testing a wide class of models and are not restricted to specific parameter values, it should be kept in mind that the dedicated analyses carried out in Ref. [5] for certain benchmark scenarios have a higher statistical sensitivity than the limits obtained from the topological cross sections. This is in particular the case in parameter regions where two (or more) channels have a similar statistical sensitivity, since the method based on the topological cross section limits allows one only to use one channel at a time.

## 6 Numerical results

In our numerical analysis we use the parameter values of the CPX benchmark scenario [7], adapted to the latest experimental central value of the top-quark mass [28] and using an on-shell value for the absolute value of the trilinear couplings  $A_t$  and  $A_b$  that is somewhat shifted compared to the  $\overline{\text{DR}}$  value specified in Ref. [7] (see Ref. [29] for a discussion in the MSSM with real parameters). Specifically, if not indicated differently we use the following parameters (the lowest-order Higgs-sector parameters  $\tan\beta$  and  $M_{H^\pm}$  are varied; in our analysis we include  $\tan\beta$  values up to 40 and  $M_{H^\pm}$  values up to 1000 GeV.)

$$\begin{aligned} M_{\text{SUSY}} &= 500 \text{ GeV}, \quad |A_t| = |A_b| = 900 \text{ GeV}, \quad \mu = 2000 \text{ GeV}, \quad m_{\tilde{g}} \equiv |M_3| = 1000 \text{ GeV}, \\ m_t &= 170.9 \text{ GeV}, \quad M_2 = 200 \text{ GeV}, \end{aligned} \tag{23}$$

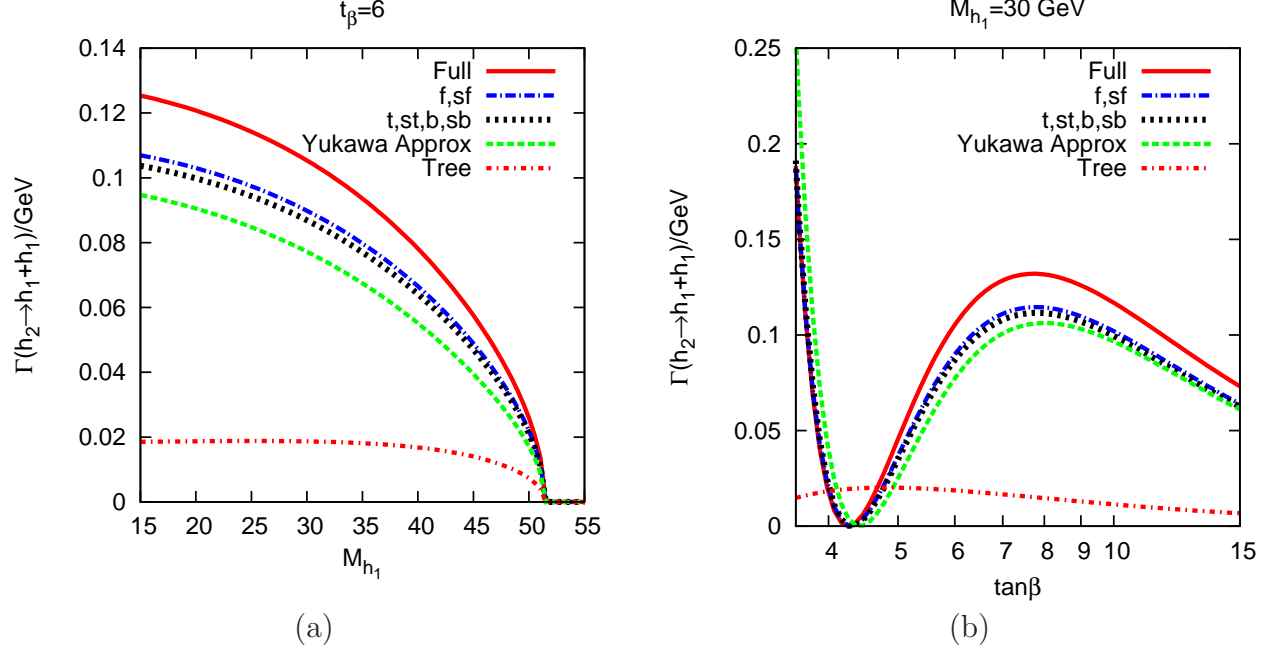


Figure 2: Full result for  $\Gamma(h_2 \rightarrow h_1 h_1)$  compared with various approximations, see text. (a)  $\Gamma(h_2 \rightarrow h_1 h_1)$  vs.  $M_{h_1}$  for  $\tan \beta = 6$  ( $M_{H^\pm}$  is varied; all other parameters are set to the CPX values given in Eqs. (23), (24)). (b)  $\Gamma(h_2 \rightarrow h_1 h_1)$  as function of  $\tan \beta$  for  $M_{h_1} = 30$  GeV ( $M_{H^\pm}$  is adjusted to ensure  $M_{h_1} = 30$  GeV).

and the complex phases of the trilinear couplings  $A_t$ ,  $A_b$  and the gluino mass parameter  $M_3$  are set to

$$\varphi_{A_t} = \frac{\pi}{2}, \quad \varphi_{A_b} = \frac{\pi}{2}, \quad \varphi_{\tilde{g}} = \frac{\pi}{2}. \quad (24)$$

In Eq. (23)  $M_{\text{SUSY}}$  denotes the diagonal soft SUSY-breaking parameters in the sfermion mass matrices that are chosen to be equal to each other,  $M_{\text{SUSY}} = M_L = M_{\tilde{q}_R}$ , see Eq. (1).

## 6.1 Results for the $h_2 \rightarrow h_1 h_1$ decay width

Fig. 2 shows the relative effect of different contributions to the  $h_2 \rightarrow h_1 h_1$  decay width in the area of the cMSSM parameter space which is particularly relevant to an investigation of the unexcluded regions in the LEP Higgs searches [5]. In Fig. 2 (a) the full result for the decay width and various approximations are plotted against  $M_{h_1}$  while keeping  $\tan \beta = 6$ . All the results plotted include the higher-order corrected wave-function normalisation factors as described in Sects. 3 and 4. They differ only in the genuine contributions to the  $h_2 h_1 h_1$  vertex. One can see that the full result (denoted as ‘Full’) differs drastically from the case where only wave-function normalisation factors but no genuine one-loop vertex contributions are taken into account (‘Tree’). The inclusion of the genuine vertex corrections that have been evaluated in this paper can increase the decay width by more than a factor of six in this example (for values of  $M_{h_1}$  sufficiently below the kinematic limit of  $M_{h_1} = 0.5 M_{h_2}$  where the decay width goes to zero). The Yukawa approximation agrees much better with the full result, giving rise to deviations of up to  $\sim 30\%$ . Using the full contribution from the  $t, \tilde{t}, b, \tilde{b}$

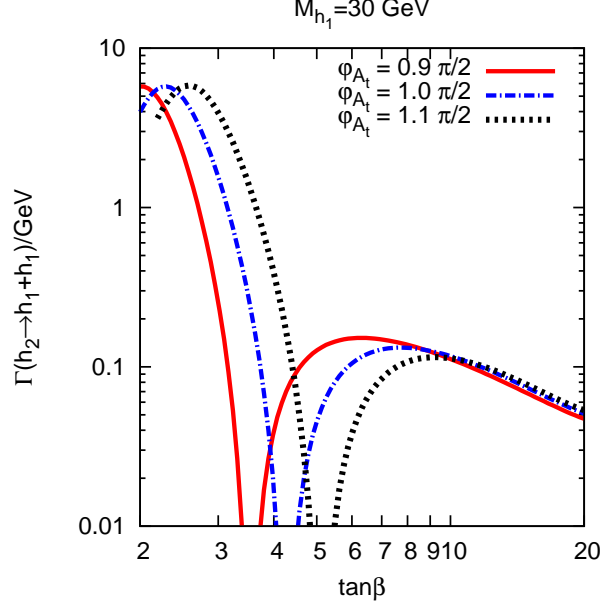


Figure 3:  $\Gamma(h_2 \rightarrow h_1 h_1)$  as function of  $\tan \beta$  for  $M_{h_1} = 30$  GeV and different values of  $\varphi_{A_t}$  ( $M_{H^\pm}$  is adjusted to ensure  $M_{h_1} = 30$  GeV).

sector ('t, st, b, sb') and from all three generations of fermions and sfermions ('f, sf') yields a prediction that deviates from the full result by up to 20%.

In Fig. 2 (b), the decay width is plotted against  $\tan \beta$  whilst adjusting  $M_{H^\pm}$  such that  $M_{h_1} = 30$  GeV. The meaning of the various lines is the same as in Fig. 2 (a). The result where the genuine vertex corrections are neglected ('Tree') shows a completely different qualitative behaviour and differs drastically from the full result. The pronounced dependence on  $\tan \beta$ , giving rise in particular to a region where  $\Gamma(h_2 \rightarrow h_1 h_1) \approx 0$  for  $\tan \beta \approx 4.3$ , is due to the fact that the Yukawa vertex corrections (which are dominant) to the matrix element change sign when  $\tan \beta$  is varied. As the decay width depends on the absolute value squared of the matrix element, the region where the Yukawa vertex corrections are close to zero corresponds to a minimum of the decay width. The deviations between the full result and the contribution from only the fermion and sfermion sector reach about 15% in this example.

In Fig. 3 the full result for  $\Gamma(h_2 \rightarrow h_1 h_1)$  is shown as a function of  $\tan \beta$  for  $M_{h_1} = 30$  GeV (adjusting  $M_{H^\pm}$  accordingly) and different values of  $\varphi_{A_t}$ . The dependence on  $\varphi_{A_t}$  is very pronounced, leading in particular to a relative shift of the curves in  $\tan \beta$ . As a consequence, comparing the results for  $\Gamma(h_2 \rightarrow h_1 h_1)$  for different values of  $\varphi_{A_t}$  at fixed values of  $\tan \beta$  can yield dramatic effects. Thus, a thorough treatment of the phase dependence is indispensable for a meaningful theoretical prediction of Higgs cascade decays in this parameter region.

## 6.2 Analysis of exclusions bounds from the LEP Higgs searches

In Figs. 4 and 5 the  $M_{h_1}$ - $\tan \beta$  parameter space of the CPX scenario is analysed. Fig. 4 shows the branching ratio of the Higgs cascade decay,  $\text{BR}(h_2 \rightarrow h_1 h_1)$ . It can be seen that, over a large part of the parameter space where the decay  $h_2 \rightarrow h_1 h_1$  is kinematically possible,

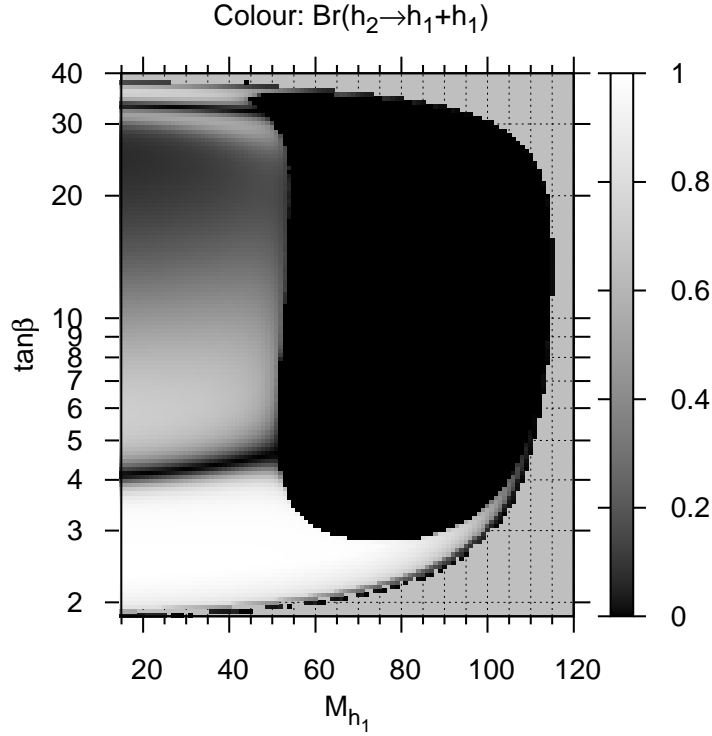


Figure 4: The branching ratio  $\text{BR}(h_2 \rightarrow h_1 h_1)$  in the  $M_{h_1}$ - $\tan \beta$  plane of the CPX scenario.

it is actually the dominant decay channel. The branching ratio is particularly large for low and moderate values of  $\tan \beta$ . In the region where  $\tan \beta \approx 4-5$  the Yukawa contribution to the matrix element for the  $h_2 \rightarrow h_1 h_1$  decay changes sign and causes a sharp drop in the  $h_2 \rightarrow h_1 h_1$  branching ratio, as was already observed in Fig. 2. A similar behaviour occurs also in the region of  $\tan \beta \approx 35$ .

Plot (a) of Fig. 5 indicates which channel has the highest statistical sensitivity and therefore which channel will be used to set an exclusion limit in different regions of the parameter space. As explained in Sect. 5, this information is needed for an interpretation of the topological cross section limits obtained at LEP [4,5] as 95% C.L. excluded regions in the  $M_{h_1}$ - $\tan \beta$  parameter space. One can see in the figure that the channels  $e^+e^- \rightarrow h_2 Z \rightarrow h_1 h_1 Z \rightarrow b\bar{b}b\bar{b}Z$  and  $e^+e^- \rightarrow h_2 h_1 \rightarrow h_1 h_1 h_1 \rightarrow b\bar{b}b\bar{b}b\bar{b}$  have the highest search sensitivity in a region with small  $M_{h_1}$  and moderate values of  $\tan \beta$ ,  $5 \lesssim \tan \beta \lesssim 9$ . For small  $M_{h_1}$  and somewhat higher  $\tan \beta$  the channel  $e^+e^- \rightarrow (h_2 h_1) \rightarrow (b\bar{b}b\bar{b})$  has the highest search sensitivity. It should be noted that all channels involving the decay of the  $h_2$  boson in the region of small  $M_{h_1}$  are strongly influenced by the  $\Gamma(h_2 \rightarrow h_1 h_1)$  decay width, either directly in the case of the channels involving the Higgs cascade decay, or indirectly through the branching ratio of the  $h_2$ . The parameter region where  $\Gamma(h_2 \rightarrow h_1 h_1)$  is important coincides with the region of the CPX scenario that could not be excluded at the 95% C.L. in the analysis of the four LEP collaborations [5].

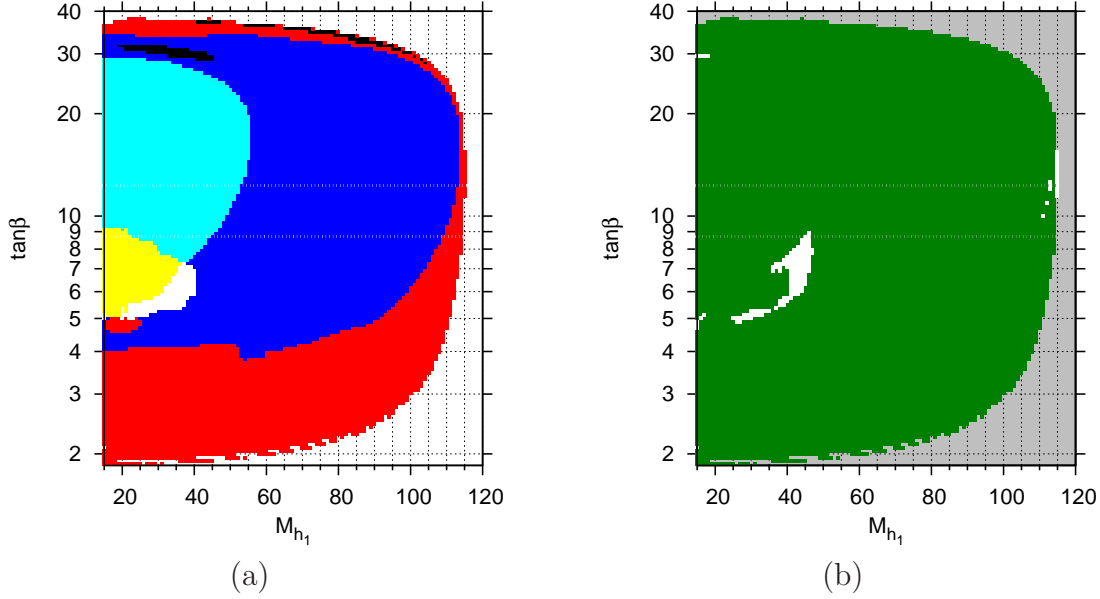


Figure 5: Coverage of the LEP Higgs searches in the  $M_{h_1}$ – $\tan\beta$  plane of the CPX scenario. Plot (a) shows the channels that are predicted to have the highest statistical sensitivity for setting an exclusion limit. The colour codings in are: red (■) =  $(h_1 Z) \rightarrow (b\bar{b}Z)$ , blue (■) =  $(h_2 Z) \rightarrow (b\bar{b}Z)$ , white (□) =  $(h_2 Z) \rightarrow (h_1 h_1 Z) \rightarrow (b\bar{b}b\bar{b}Z)$ , cyan (■) =  $(h_2 h_1) \rightarrow (b\bar{b}b\bar{b})$ , yellow (■) =  $(h_2 h_1) \rightarrow (h_1 h_1 h_1) \rightarrow (b\bar{b}b\bar{b}b\bar{b})$ , black (■) = other channels. Plot (b) shows the parameter regions excluded at the 95% C.L. by the topological cross section limits obtained at LEP [4, 5]. The colour codings are: green (dark grey) = LEP excluded, white = LEP allowed.

In plot (b) of Fig. 5 we have combined our new theoretical predictions (containing the complete one-loop result for the genuine vertex corrections and higher-order corrections, as described above) with the topological cross section limits obtained at LEP. We find an unexcluded region at  $M_{h_1} \approx 45$  GeV and moderate  $\tan\beta$  where channels involving the decay  $h_2 \rightarrow h_1 h_1$  play an important role. Thus, our analysis, based on the most up-to-date theory prediction for the  $h_2 \rightarrow h_1 h_1$  channel, confirms the ‘hole’ in the LEP coverage observed in Ref. [5] (see in particular Fig. 19 of Ref. [5]).

It should be noted, on the other hand, that the results shown in plot (b) of Fig. 5 differ in several respects from the results presented in Ref. [5]. As discussed above, near to borders between areas where different search topologies are predicted to have the highest exclusion power our analysis has less statistical sensitivity than the benchmark studies of Ref. [5]. A further difference is the input value of the top-quark mass. While we are using the latest experimental central value of  $m_t = 170.9$  GeV [28], most of the analysis of Ref. [5] was done for  $m_t = 174.3$  GeV. We have explicitly checked that (as expected) the unexcluded region is significantly increased if we use  $m_t = 174.3$  GeV instead. Concerning differences in the theoretical predictions, the analysis of Ref. [5] was based on the two codes *FeynHiggs2.0*, an earlier version of the *FeynHiggs* program [18], and *CPH* [7], a predecessor of the program *CPsuperH* [19]. For each scan point, in Ref. [5] the results from *CPH* and *FeynHiggs2.0* (for the decay width  $\Gamma(h_2 \rightarrow h_1 h_1)$  the *CPH* formula was used in both codes) were compared with each other, and the result yielding the more conservative exclusion bound was retained.

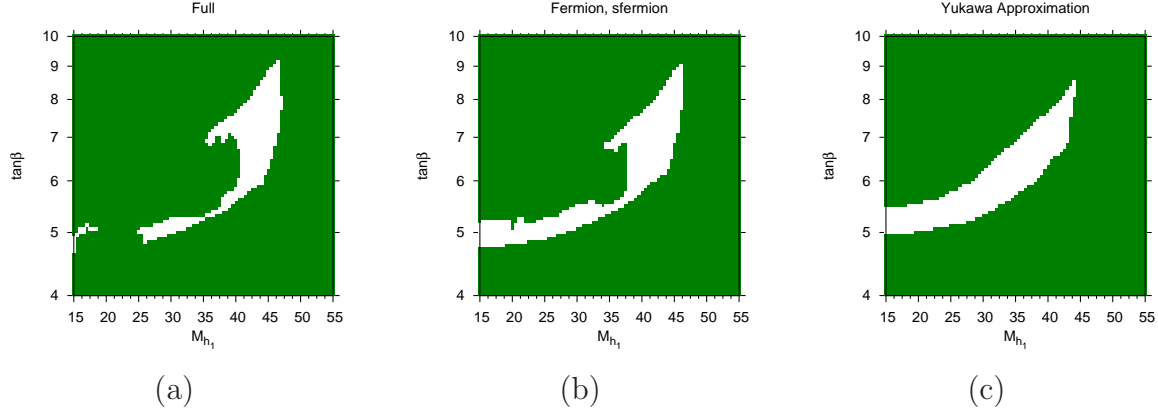


Figure 6: Impact of the genuine vertex corrections on the ‘hole’ in the LEP coverage for  $M_{h_1} \approx 45$  GeV and  $\tan \beta \approx 7$ . Plot (a) shows the full result (detailed view of plot (b) of Fig. 5). Plot (b) shows the result for the case where only contributions from SM fermions and their superpartners are taken into account in the genuine vertex corrections. Plot (c) shows the result where the Yukawa Approximation has been used for the genuine vertex corrections. The colour codings are: green (dark grey) = LEP excluded, white = LEP allowed.

Our theoretical prediction for  $\Gamma(h_2 \rightarrow h_1 h_1)$  based on a complete diagrammatic one-loop result of the genuine vertex contribution goes significantly beyond the effective coupling approximation used in Ref. [5]. Furthermore, the  $\mathcal{O}(\alpha_t \alpha_s)$  propagator-type corrections obtained in the Feynman-diagrammatic approach for arbitrary complex phases [15] were not yet available when the analysis of Ref. [5] was carried out.

In Fig. 6 we focus on the uncovered parameter region at  $M_{h_1} \approx 45$  GeV and  $\tan \beta \approx 7$  and compare our complete one-loop result for the genuine triple-Higgs vertex corrections with two approximations. While plot (a) shows the full result (i.e., it is a detailed view of plot (b) of Fig. 5), in plot (b) the genuine vertex corrections are approximated by the contributions from fermions and sfermions only, and in plot (c) the Yukawa Approximation has been used for the genuine vertex corrections. In all three plots the wave function normalisation factors and all other decay widths are the same (calculated as described above). The differences between the three plots in Fig. 6 are therefore entirely caused by the genuine vertex corrections to the Higgs cascade decays. While all three graphs show an unexcluded region at  $M_{h_1} \approx 45$  GeV and  $\tan \beta \approx 7$ , the shape of this region changes quite significantly. In particular, the analysis based on the full result gives rise to a considerably larger unexcluded region around  $M_{h_1} \approx 45$  GeV and  $\tan \beta \approx 7$  compared to the Yukawa Approximation (while the Yukawa Approximation gives rise to a larger unexcluded region for smaller  $M_{h_1}$ ). As expected from Fig. 2, the inclusion of all SM fermion and sfermion loop contributions yields a better approximation of the full result.

## 7 Conclusions

We have obtained, within the MSSM with complex parameters, complete one-loop results for the classes of decay processes in which a heavier neutral Higgs boson decays into two lighter

ones and for those in which a neutral Higgs boson decays into a pair of SM fermions. Our results take into account all sectors of the MSSM and incorporate the full dependence on all complex phases of the supersymmetric parameters and the external momenta. The new one-loop results have been supplemented with state-of-the-art propagator-type corrections containing higher-order contributions obtained in the FD approach (taken from the program *FeynHiggs*), yielding in this way the currently most precise predictions for these processes within the MSSM with complex parameters.

We find that the genuine vertex contributions to the triple-Higgs vertex are numerically very important. Their inclusion changes the predictions for the decay widths very drastically compared to the case of an effective coupling approximation based only on the wave function normalisation factors of the external Higgs bosons. Including genuine vertex corrections in a simple Yukawa Approximation yields a prediction for the decay width that is much closer to the full result, but we still find deviations of up to 30% in the numerical examples investigated in this paper (using the CPX scenario). Even contributions beyond the fermion/sfermion sector can have a sizable impact on the decay widths. We have furthermore found that the dependence of the decay width on the complex phase  $\varphi_{A_t}$  is very pronounced, emphasizing the need for a thorough treatment of the effects of complex phases.

Based on our improved theoretical predictions we have analysed the impact of the limits on topological cross sections obtained from the LEP Higgs searches on the parameter space with a very light Higgs boson within the MSSM with complex parameters. We find that, over a large part of the parameter space where the decay  $h_2 \rightarrow h_1 h_1$  is kinematically possible, it is the dominant decay channel. The corresponding search channels  $e^+ e^- \rightarrow h_2 Z \rightarrow h_1 h_1 Z \rightarrow b\bar{b}b\bar{b}Z$  and  $e^+ e^- \rightarrow h_2 h_1 \rightarrow h_1 h_1 h_1 \rightarrow b\bar{b}b\bar{b}b\bar{b}$  have the highest sensitivity for setting an exclusion limit in a region with small  $M_{h_1}$  and moderate values of  $\tan\beta$ . We find that a parameter region with  $M_{h_1} \approx 45$  GeV and  $\tan\beta \approx 7$  remains unexcluded by the limits on topological cross sections obtained from the LEP Higgs searches, confirming the results of the four LEP collaborations achieved in a dedicated analysis of the CPX benchmark scenario. A precise theory prediction for the  $h_2 \rightarrow h_1 h_1$  channel is crucial for mapping out the unexcluded parameter region (it should be noted in this context that in the parameter region of the CPX scenario also formally sub-leading two-loop corrections can have a sizable numerical impact). We find that the shape of the unexcluded region is significantly modified if the full result for the vertex corrections is replaced by approximations.

The results presented in this paper will be included in the public code *FeynHiggs*. It would be interesting to compare our results with the other public code for evaluating Higgs masses and decay widths in the MSSM with complex parameters, *CPsuperH*. This comparison is affected, however, not only by the genuine triple-Higgs vertex corrections that are the main focus of the present paper, but also by differences in the propagator-type corrections used in the two codes. Furthermore, a meaningful comparison between *FeynHiggs* and *CPsuperH* requires a translation between the on-shell input parameters used in *FeynHiggs* and the  $\overline{\text{DR}}$  input parameters used in *CPsuperH*. Such a detailed comparison is beyond the scope of the present paper. We will address this issue in a forthcoming publication.



## Acknowledgements

We thank P. Bechtle, O. Brein, T. Hahn, S. Heinemeyer, W. Hollik, S. Palmer, A. Read, H. Rzehak and D. Stöckinger for numerous helpful discussions. Collaboration with P. Bechtle, O. Brein and S. Heinemeyer on the implementation of the bounds from the LEP Higgs searches into the code *HiggsBounds* is gratefully acknowledged. Work supported in part by the European Community's Marie-Curie Research Training Network under contract MRTN-CT-2006-035505 'Tools and Precision Calculations for Physics Discoveries at Colliders'.

## References

- [1] V. Büscher and K. Jakobs, *Int. J. Mod. Phys. A* **20** (2005) 2523, hep-ph/0504099.
- [2] A. Djouadi et al. [ILC Global Design Effort and World Wide Study], arXiv:0709.1893 [hep-ph].
- [3] E. Accomando et al. [CLIC Physics Working Group], hep-ph/0412251.
- [4] [LEP Higgs working group], *Phys. Lett. B* **565** (2003) 61, hep-ex/0306033;
- [5] [LEP Higgs working group], *Eur. Phys. J. C* **47** (2006) 547, hep-ex/0602042.
- [6] M. Carena, S. Heinemeyer, C. Wagner and G. Weiglein, hep-ph/9912223; *Eur. Phys. J. C* **26** (2003) 601, hep-ph/0202167.
- [7] M. Carena, J. Ellis, A. Pilaftsis and C. Wagner, *Phys. Lett.* **495** (2000) 155, hep-ph/0009212.
- [8] M. Schumacher, *Czech. J. Phys.* **54** (2004) A103; hep-ph/0410112.
- [9] E. Accomando et al., hep-ph/0608079.
- [10] P. Bandyopadhyay, A. Datta, A. Datta and B. Mukhopadhyaya, arXiv:0710.3016 [hep-ph].
- [11] S. Heinemeyer and W. Hollik, *Nucl. Phys. B* **474** (1996) 32, hep-ph/9602318.
- [12] R. Dermisek and J.F. Gunion, *Phys. Rev. Lett.* **95** (2005) 041801, hep-ph/0502105.
- [13] A. Pilaftsis, *Phys. Lett. B* **435** (1998) 88, hep-ph/9805373;  
S. Heinemeyer, *Eur. Phys. J. C* **22** (2001) 521, hep-ph/0108059.
- [14] M. Frank, T. Hahn, S. Heinemeyer, W. Hollik, H. Rzehak and G. Weiglein, *JHEP* **02** (2007) 047, hep-ph/0611326.
- [15] S. Heinemeyer, W. Hollik, H. Rzehak and G. Weiglein, *Phys. Lett. B* **652** (2007) 300, arXiv:0705.0746 [hep-ph]; *AIP Conf. Proc.* **903** (2007) 149.

- [16] D. Demir, *Phys. Rev. D* **60** (1999) 055006, hep-ph/9901389;  
A. Pilaftsis and C. Wagner, *Nucl. Phys. B* **553** (1999) 3, hep-ph/9902371;  
S. Choi, M. Drees and J. Lee, *Phys. Lett. B* **481** (2000) 57, hep-ph/0002287;  
M. Carena, J. Ellis, A. Pilaftsis and C. Wagner, *Nucl. Phys. B* **586** (2000) 92, hep-ph/0003180;  
T. Ibrahim and P. Nath, *Phys. Rev. D* **63** (2001) 035009, hep-ph/0008237; *Phys. Rev. D* **66** (2002) 015005, hep-ph/0204092;  
S. Martin, *Phys. Rev. D* **67** (2003) 095012, hep-ph/0211366; *Phys. Rev. D* **71** (2005) 016012, hep-ph/0405022; *Phys. Rev. D* **75** (2007) 055005, hep-ph/0701051.
- [17] S. Heinemeyer, W. Hollik and G. Weiglein, *Phys. Rev. D* **58** (1998) 091701, hep-ph/9803277; *Phys. Lett. B* **440** (1998) 296, hep-ph/9807423; *Eur. Phys. J. C* **9** (1999) 343, hep-ph/9812472;  
M. Frank, S. Heinemeyer, W. Hollik and G. Weiglein, hep-ph/0212037, in the proceedings of *SUSY02*, July 2002, DESY, Hamburg, Germany;  
G. Degrandi, S. Heinemeyer, W. Hollik, P. Slavich and G. Weiglein, *Eur. Phys. J. C* **28** (2003) 133, hep-ph/0212020.
- [18] S. Heinemeyer, W. Hollik and G. Weiglein, *Comput. Phys. Commun.* **124** (2000) 76, hep-ph/9812320; hep-ph/0002213; see [www.feynhiggs.de](http://www.feynhiggs.de).
- [19] J.S. Lee, A. Pilaftsis, M. Carena, S.Y. Choi, M. Drees, J. Ellis and C.E.M. Wagner, *Comput. Phys. Commun.* **156** (2004) 283, hep-ph/0307377;  
J.S. Lee, M. Carena, J. Ellis, A. Pilaftsis and C.E.M. Wagner, arXiv:0712.2360 [hep-ph].
- [20] J. Küblbeck, M. Böhm and A. Denner, *Comput. Phys. Commun.* **60** (1990) 165;  
T. Hahn, *Comput. Phys. Commun.* **140** (2001) 418, hep-ph/0012260;  
T. Hahn and C. Schappacher, *Comput. Phys. Commun.* **143** (2002) 54, hep-ph/0105349.  
The program and the user's guide are available via [www.feynarts.de](http://www.feynarts.de).
- [21] T. Hahn and M. Pérez-Victoria, *Comput. Phys. Commun.* **118** (1999) 153, hep-ph/9807565.
- [22] T. Hahn, S. Heinemeyer, W. Hollik, H. Rzehak, G. Weiglein and K.E. Williams, hep-ph/0611373.
- [23] T. Hahn, S. Heinemeyer, W. Hollik, H. Rzehak, G. Weiglein and K.E. Williams, arXiv:0711.2020 [hep-ph].
- [24] A. Brignole, G. Degrandi, P. Slavich and F. Zwirner, *Nucl. Phys. B* **631** (2002) 195, hep-ph/0112177; *Nucl. Phys. B* **643** (2002) 79, hep-ph/0206101;  
J. Espinosa and R. Zhang, *Nucl. Phys. B* **586** (2000) 3, hep-ph/0003246;  
G. Degrandi, A. Dedes and P. Slavich, *Nucl. Phys. B* **672** (2003) 144, hep-ph/0305127;  
S. Heinemeyer, W. Hollik, H. Rzehak and G. Weiglein, *Eur. Phys. J. C* **39** (2005) 465, hep-ph/0411114.
- [25] P. Bechtle and A. Read, private communications.

- [26] P. Bechtle et al., in preparation.
- [27] O. Brein and T. Hahn, *Eur. Phys. J. C* **52** (2007) 397, hep-ph/0610079;  
O. Brein and W. Hollik, *Phys. Rev. D* **76** (2007) 035002, arXiv:0705.2744 [hep-ph].
- [28] Tevatron Electroweak Working Group, hep-ex/0703034.
- [29] M. Carena, H. Haber, S. Heinemeyer, W. Hollik, C. Wagner, and G. Weiglein, *Nucl. Phys. B* **580** (2000) 29, hep-ph/0001002.